

# **EFFECT OF SIMULATED THERMOMECHANICAL PROCESSING ON THE TRANSFORMATION CHARACTERISTICS AND MICROSTRUCTURE OF AN API X80 PIPELINE STEEL**

Pavel Cizek, Brad P. Wynne – University of Sheffield, United Kingdom

Peter D. Hodgson – Deakin University, Australia

Barry C. Muddle – Monash University, Australia

## **ABSTRACT**

The transformation behaviour and microstructural characteristics of the transformation products were studied in an API X80 pipeline steel subjected to simulated controlled rolling followed by controlled cooling. Deformation dilatometry was employed to investigate the transformation characteristics of both recrystallised and heavily deformed austenite during cooling at rates from 0.1°C/s to about 100°C/s and the corresponding CCT diagrams were constructed. The transformation product microstructures were studied in detail using optical, scanning electron, and transmission electron microscopy, complemented by automatic image analysis. The detailed transformation and microstructural characteristics, obtained in the present work, could be used for the optimisation of thermomechanical processing schedules for API X80 and similar higher-grade pipeline steels.

## **KEYWORDS**

Austenite, bainite, CCT diagram, deformation dilatometry, ferrite, microstructure, pipeline steel

## **INTRODUCTION**

A constantly increasing demand of the pipeline industry for a more cost-effective pipeline design has pushed the standard pipeline steel grade requirements up to API X80 and beyond. Critical to the design of these steels is a low carbon equivalent for good field weldability [1]. To compensate for the loss in strength, additions of microalloying elements such as niobium, titanium and molybdenum are used. These additions contribute to an increase in strength both directly, through microstructural refinement, solid solution strengthening and precipitation hardening, as well as indirectly, through enhanced hardenability and associated modification of the resultant transformation microstructures [1,2]. Optimum product microstructures, with a desired balance of mechanical properties at a given steel composition, are being achieved through suitably designed thermomechanical processing schedules [2], which commonly involve controlled rolling followed by controlled accelerated cooling. The controlled rolling step usually includes heavy deformation of the austenite, carried out in the non-recrystallisation temperature region, which brings about significant refinement of the final transformation microstructures. The accelerated cooling step aims to suppress the formation of polygonal ferrite and, instead, encourage non-equilibrium, non-equiaxed ferrite microstructures to be formed. The latter transformation products are known to contribute to increasing strength, through both small effective grain sizes and increased dislocation densities, while maintaining a reasonable level of toughness [1-3]. The non-equilibrium ferrite microstructures do not contain cementite and possess some unique morphological features.

A specific terminology [4] has been adopted in the present work in an attempt to describe all possible ferrite morphologies formed by the decomposition of austenite in these modern

microalloyed steels with very low carbon contents. Apart from martensite (M), this terminology recognizes five separate forms of ferrite: (i) polygonal ferrite (PF), the equilibrium microstructural constituent characterized by roughly equiaxed grains with smooth boundaries, mostly containing a low dislocation density and no substructure; (ii) Widmanstätten ferrite (WF), defined by elongated crystals of ferrite with dislocation substructure; (iii) quasi-polygonal ferrite (QF), characterized by grains with undulating boundaries containing dislocation substructure and occasional martensite-austenite (M/A) micro-constituent; (iv) granular ferrite (GF), which consists of sheaves of elongated ferrite crystals with low misorientations and a high dislocation density, containing roughly equiaxed islands of M/A micro-constituent; and (v) bainitic ferrite (BF), which consists of packets of parallel ferrite laths (or plates) separated by low-angle boundaries and containing very high dislocation densities. In contrast to GF, the M/A micro-constituent retained between the ferrite crystals in BF has an acicular morphology. The austenite decomposition products containing cementite are generally classified as pearlite (P), degenerate pearlite (P') and "classical" bainite (B). In order to differentiate between conventional upper bainite (UB) and lower bainite (LB), the classification scheme proposed by Ohmori et al. [5] has been adopted.

In order to obtain greater understanding of the processes that take place during industrial processing of a modern API X80 linepipe steel, the aim of the present work was to characterise the transformation behaviour and microstructures developed in this steel during laboratory simulation of controlled rolling in conjunction with controlled continuous cooling.

## 1. EXPERIMENTAL PROCEDURES

The chemical composition of the steel studied was 0.065 mass% C, 0.29% Si, 1.55% Mn, 0.015% P, 0.003% S, 0.036% Al, 0.28% Mo, 0.076% Nb, 0.020% Ti, and the balance Fe. The steel was supplied by the Bluescope Steel, Australia. Deformation dilatometry was performed using a computerised high-speed quenching and deformation dilatometer. The dilatometry specimens were solid cylinders with a diameter of 4 mm and a length of 8 mm. The specimens were subjected to the simulated recrystallisation and non-recrystallisation rolling schedules (Fig. 1), followed by controlled cooling at rates from 0.1°C/s to approximately 100°C/s. Both rolling schedules included a simulated "roughing" step performed at a temperature of 1100°C using a strain of 0.30, followed by post-deformation holding at the above temperature for 120 s to ensure complete recrystallisation. The simulated non-recrystallisation rolling schedule contained an additional "finishing" step performed at a temperature of 875°C, which was situated in the non-recrystallisation temperature region, using a strain of 0.47 in compression. The cooling rates were defined by the time interval required for the specimens to cool from 800°C to 500°C. The mean grain diameter of the initial austenite was about 40 µm. All specimens were Vickers hardness tested using a 5 kg load and examined by both optical and scanning electron microscopy in conjunction with automatic image analysis after being etched with 2% nital. The information obtained was used to construct continuous cooling transformation (CCT) diagrams. A more detailed metallographic examination was performed on selected specimens using transmission electron microscopy (TEM).

## 2. RESULTS

### 2.1. TRANSFORMATION BEHAVIOUR

The CCT diagrams obtained are presented in Fig. 2. In the case of transformation from the recrystallised austenite (Fig. 2a), the presence of PF within the resulting transformation

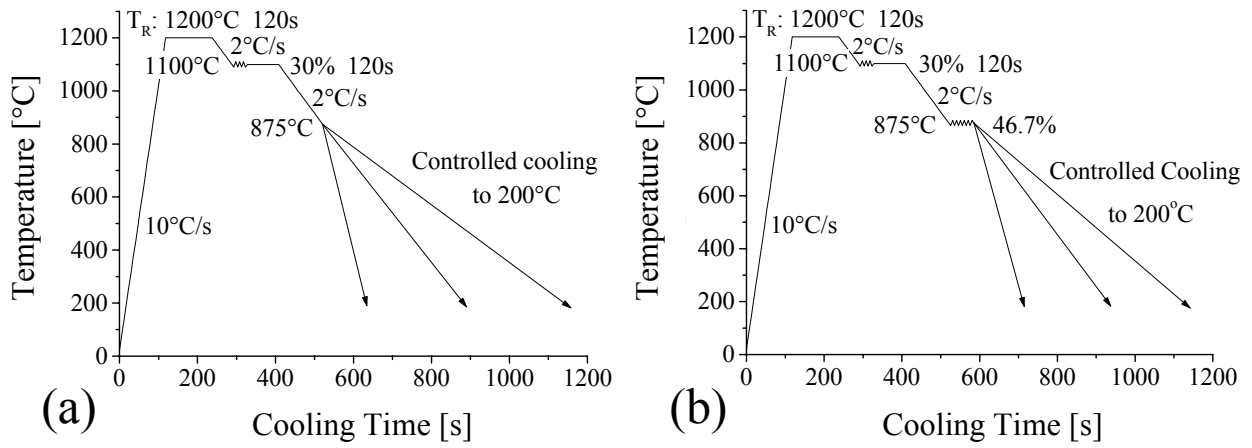


Fig. 1. Schematics of the simulated rolling schedules: (a) recrystallisation schedule; (b) non-recrystallisation schedule.

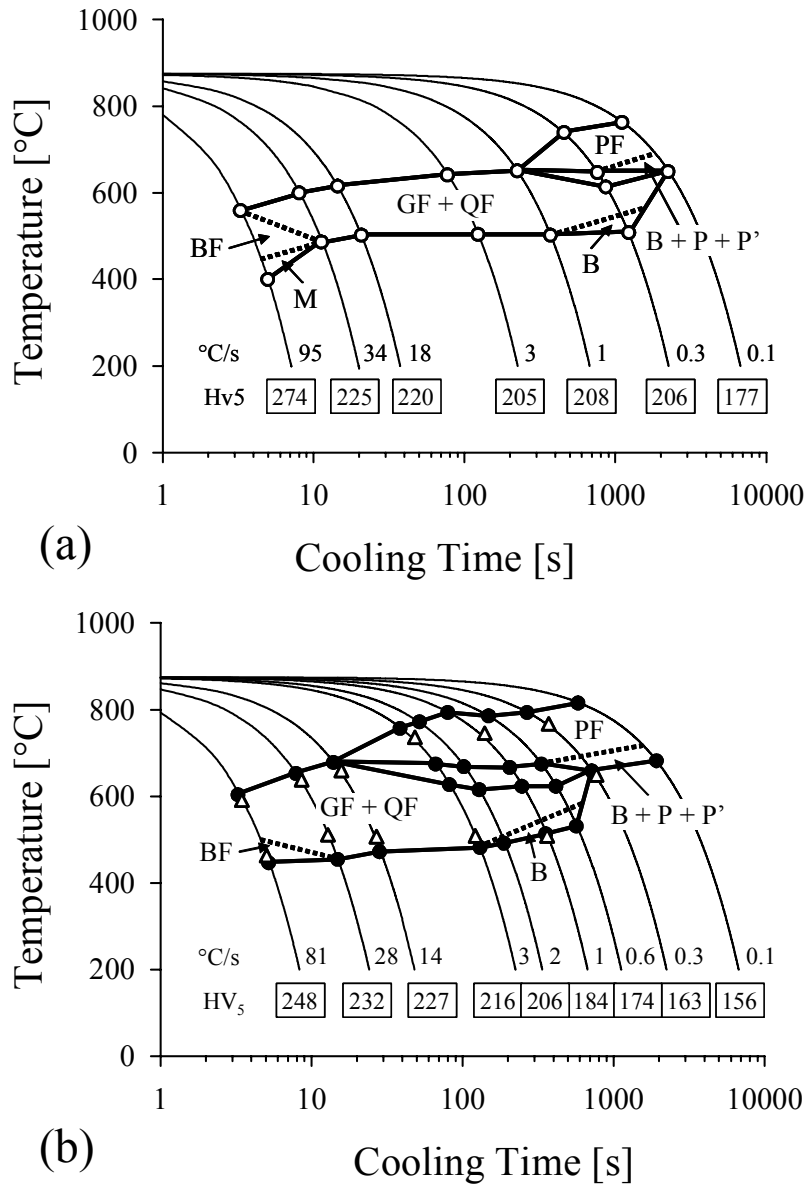


Fig. 2. CCT diagrams obtained for the recrystallised (a) and deformed (b) austenite.

microstructure was restricted to the cooling rates below approximately  $1^{\circ}\text{C/s}$ . At a cooling rate of  $0.3^{\circ}\text{C/s}$ , PF formation was followed by the conversion of the remaining untransformed austenite into GF. The formation of a mix of QF and GF was observed to spread over a wide interval of cooling rates ranging from  $1^{\circ}\text{C/s}$  up to  $34^{\circ}\text{C/s}$ . At a cooling rate of  $95^{\circ}\text{C/s}$ , the transformation microstructure was dominated by BF accompanied by a small amount of M. Heavy deformation of the prior austenite brought about a significant expansion of the PF transformation field in the CCT diagram at the expense of a mix of QF and GF (Fig. 2b). The corresponding transformation start temperatures underwent a noticeable increase, as illustrated by the deviations of the transformation points (marked by solid circles) from the superimposed open triangles. The transformation temperatures represented by the triangles were derived from the CCT diagram of the recrystallised austenite at roughly comparable microstructures. Following the same way of comparison, the transformation start temperatures of a mix of QF and GF were found to increase slightly, whereas the corresponding transformation finish temperatures underwent a marginal decrease. This brought about slight widening of the corresponding temperature interval of transformation. Also, as a result of the austenite deformation, the formation of BF was noticeably suppressed and that of M entirely eliminated within the studied range of cooling rates.

Measurements of the bulk Vickers hardness of each of the dilatometer specimens were superimposed on the corresponding CCT diagrams in Fig. 2. As expected, the lowest hardness values observed corresponded to the microstructures dominated by PF, which formed at the highest transformation start temperatures. Conversely, the highest hardness value was displayed by the microstructure composed of BF and martensite, forming at the lowest transformation start temperature from the recrystallised prior austenite. The hardness data obtained for QF and GF, characterised by intermediate formation temperatures, were situated between the above limits. The transformation microstructures formed from the deformed parent austenite were generally observed to display slightly increased hardness values compared to the equivalent microstructures created from the recrystallised austenitic matrix.

## 2.2. TRANSFORMATION MICROSTRUCTURES

In the following, the microstructural characteristics of the transformation products obtained from the recrystallised austenite (see Fig. 2a) will be first discussed in detail and some comments on the impact of the austenite deformation on these characteristics will be subsequently made. The microstructure of PF grains was observed to contain carbon-enriched islands comprising a complex mixture of austenite decomposition products. At the lowest cooling rate of  $0.1^{\circ}\text{C/s}$ , the carbon-enriched regions largely displayed quite uniform dark-etching contrast in optical micrographs (Fig. 3a) and TEM showed that they were predominantly composed of bainite, accompanied by a small amount of fine P or P'. The observed bainite morphology could be best classified as a mixture of BII and BIII upper bainite according to the scheme proposed by Ohmori et al. [5]. The BII sheaves were composed of highly-dislocated ferrite laths separated by continuous cementite layers, while the BIII sheaves, which were observed much more frequently than BII, contained discrete cementite platelets aligned along a common direction within the ferrite matrix (Fig. 4a). When increasing cooling rate to  $0.3^{\circ}\text{C/s}$ , PF volume fraction decreased and the rest of the microstructure became characterized by dark-etching micro-regions scattered within white ferritic areas (Fig. 3b). In the TEM, the micro-regions displaying the dark-etching response in optical micrographs were composed predominantly of bainite, with only a small fraction of fine P'. The ferrite matrix, in which the dark-etching particles were embedded, contained a high dislocation density and was subdivided into fragments separated by low-angle boundaries. Thus, such a microstructure appeared to be similar to that observed within the GF sheaves formed at higher cooling rate regimes (see

below), apart from the second-phase micro-regions being coarser and composed largely of classical bainite rather than M/A micro-constituents typical of GF.

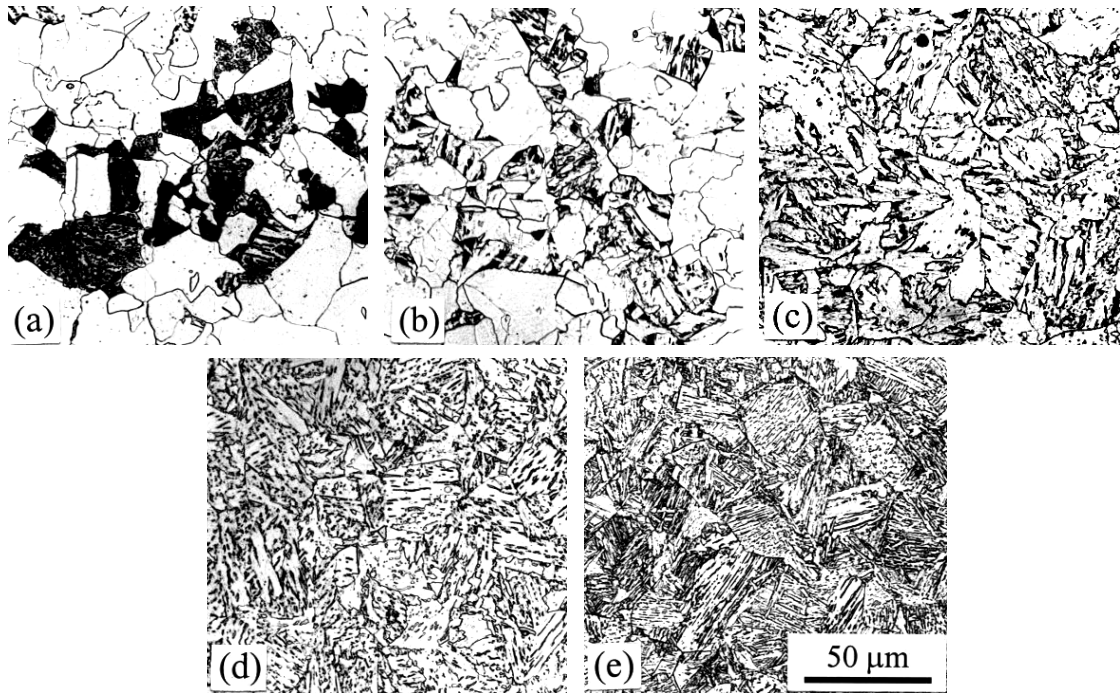


Fig.3. Optical micrographs of the microstructures transformed from the recrystallised austenite: (a) 0.1°C/s, PF+B; (b) 0.3°C/s, PF+GF; (c) 1°C/s, QF+GF; (d) 18°C/s, GF; (e) 95°C/s, BF+M.

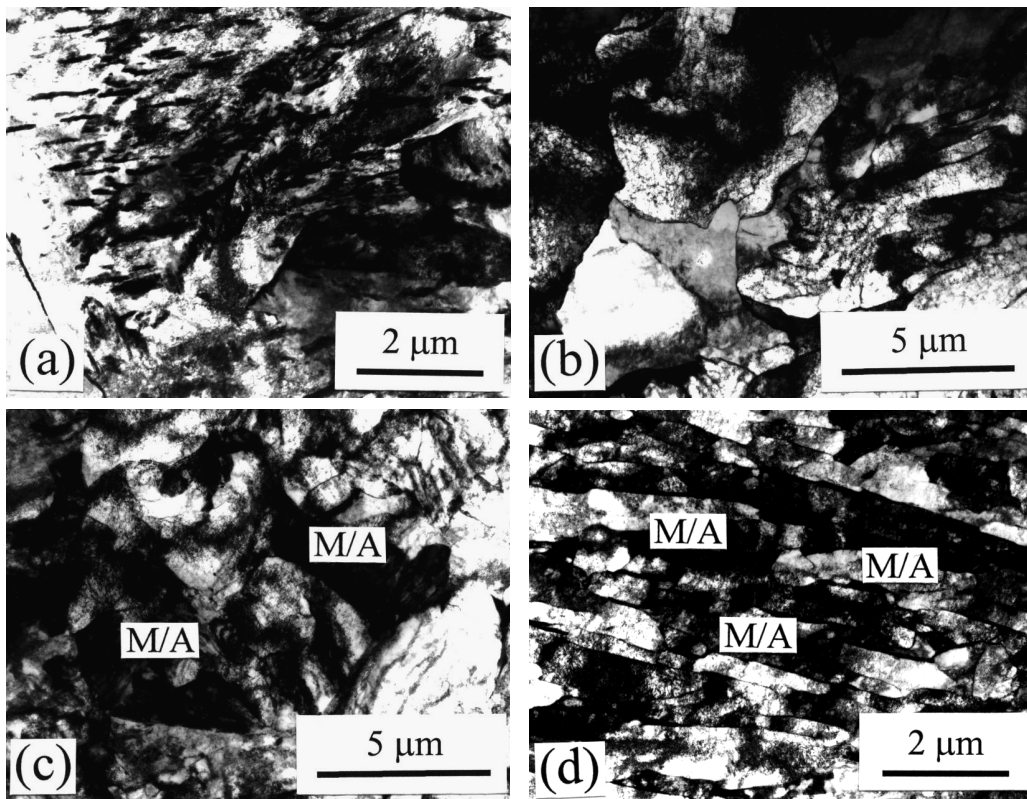


Fig. 4. TEM micrographs of the transformation products obtained from the recrystallised austenite: (a) 0.1°C/s, BII; (b) 1°C/s, QF; (c) 18°C/s, GF; (d) 95°C/s, BF.

When the cooling rate reached  $1^{\circ}\text{C/s}$ , PF ceased to be formed and the transformation microstructure became dominated by QF, accompanied by GF (Fig. 3c). For the microstructures predominantly composed of QF, there was no clear indication of the locations of prior austenite grain boundaries. The QF grains were characterised by undulating boundaries and the presence of clearly etched sub-boundaries in their interiors. These grains occasionally contained second-phase micro-regions, composed of a mixture of dark-etching classical bainite particles and grey M/A micro-constituents. TEM analysis revealed that QF grains were composed of coarse fragments, separated by low-angle boundaries and containing significant dislocation densities (Fig. 4b). A gradual increase in cooling rate was accompanied by a parallel increase in the volume fraction of GF in the microstructure, at the expense of QF, and the distributed micro-regions became dominated by M/A micro-constituents. When the microstructure contained a significant volume fraction of GF, the locations of the prior austenite grain boundaries remained largely preserved (Fig. 3d). Observed by TEM, the GF sheaves were composed of both elongated and roughly equiaxed fragments, separated by low-angle boundaries and having high internal dislocation densities, and contained approximately equiaxed regions of M/A micro-constituent (Fig. 4c). The latter comprised a number of variants of highly-dislocated lath martensite, accompanied by barely detectable retained austenite. In contrast to the substructural characteristics of QF grains, the fragments present within GF sheaves were generally finer and the corresponding dislocation densities comparatively higher. An increase in cooling rate to  $95^{\circ}\text{C/s}$  brought about a transition from GF to BF, as well as the formation of a small volume fraction of lath martensite (see Fig. 2a). In optical micrographs, BF was characterised by packets of parallel laths (or plates), containing fine acicular M/A micro-regions along their boundaries, and the locations of the original austenite boundaries remained entirely retained (Fig. 3e). The substructure of BF packets was characterised by sympathetically nucleated, nearly parallel laths separated by low-angle boundaries and containing very high dislocation densities in their interior (Fig. 4d).

The microstructures obtained after transformation from the deformed, unrecrystallised austenite essentially remained similar in character to those originated from the recrystallised austenite matrix. However, due to the austenite deformation, both the PF and QF grains became significantly refined and a similar trend was observed for the GF sheaves. The mean size of PF grains formed from the recrystallised austenite matrix reached values of about  $21\ \mu\text{m}$  and  $19\ \mu\text{m}$  at cooling rates of  $0.1^{\circ}\text{C/s}$  and  $0.3^{\circ}\text{C/s}$ , respectively. As a result of plastic deformation of the parent austenite, the average PF grain size became refined to a value of about  $7\ \mu\text{m}$  for a cooling rate of  $0.1^{\circ}\text{C/s}$ . The above PF grains formed from the deformed austenite were observed to undergo a modest gradual refinement with increasing cooling rate and they reached a mean size of about  $5\ \mu\text{m}$  at a cooling rate of  $3^{\circ}\text{C/s}$ . Results of a detailed statistical evaluation of the size of the classical bainite islands, QF grains and/or GF/BF sheaves/packets as a function of cooling rate for both the recrystallised and deformed prior austenite are summarised in Fig. 5. The obtained curves displayed a similar shape and the curve for the deformed austenite was shifted towards the lower values and higher cooling rates with respect to its counterpart corresponding to the recrystallised starting matrix. The above shift appears to reflect that displayed by the respective CCT diagrams (see Fig. 2), resulting from reduced effective hardenability of the deformed parent austenite. The observed gradual transition from the microstructures containing classical bainite islands, embedded within the PF matrix, to those composed of QF and GF with increasing cooling rate was reflected in the both curves through a progressive increase in the corresponding island/grain/sheaf dimensions. The curves started with the values of about  $9\ \mu\text{m}$  and  $8\ \mu\text{m}$  at a cooling rate of  $0.1^{\circ}\text{C/s}$  and reached a maximum at values of about  $15\ \mu\text{m}$  at a cooling rate of  $1^{\circ}\text{C/s}$  and approximately  $11\ \mu\text{m}$  at a cooling rate of  $3^{\circ}\text{C/s}$  for the recrystallised and deformed parent austenite, respectively (see Fig. 5). Further increase in cooling rate, accompanied by a gradual increase in GF volume fraction at the expense of QF and ultimately the formation of BF for the recrystallised austenite, led to a progressive decrease in GF sheaf size.

At cooling rates of around  $100^{\circ}\text{C/s}$ , the BF packet size and GF sheaf size reached values of about  $12\ \mu\text{m}$  and  $7\ \mu\text{m}$  for the recrystallised and deformed prior austenite, respectively.

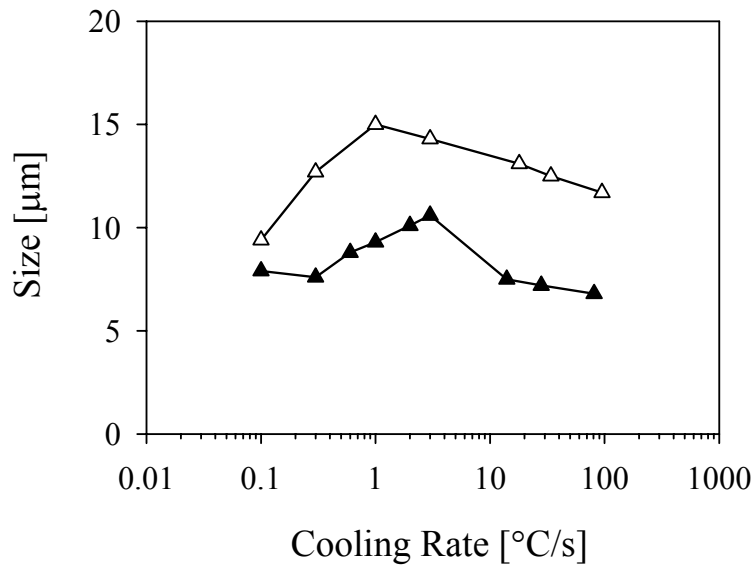


Fig. 5. Mean size of the classical bainite islands, QF grains and/or GF/BF sheaves/packets as a function of cooling rate (open and filled symbols correspond to the recrystallised and deformed prior austenite, respectively).

Results of a detailed statistical evaluation of the size, shape and volume fraction of the second-phase (classical bainite and/or M/A constituent) particles, obtained using a combination of optical and scanning electron microscopy in conjunction with automatic image analysis, are summarised in Figs. 6 and 7. The mean size of second-phase particles displayed a similar dependence on cooling rate, as well as roughly comparable values at a given cooling rate, for the both recrystallised and deformed parent austenite (Fig. 6a). These values would come even closer together if the comparison was made at similar microstructures, rather than at a given cooling rate, as the curve for the deformed starting austenite would then become shifted towards the lower cooling rates due to its reduced effective hardenability. The average size of classical bainite particles was observed to decrease from values of around  $3\ \mu\text{m}$  to those of less than  $2\ \mu\text{m}$  with an increase in cooling rate from  $0.1^{\circ}\text{C/s}$  to  $1^{\circ}\text{C/s}$ , while the mean size of M/A micro-regions decreased from values of around  $1.5\ \mu\text{m}$  to those slightly smaller than  $1\ \mu\text{m}$  with a cooling rate increase from  $1^{\circ}\text{C/s}$  to about  $100^{\circ}\text{C/s}$ . The evolution of the shape of second-phase particles with cooling rate is presented in Fig. 6b using the ellipse ratio  $a/b$ . With cooling rate increasing from  $0.1^{\circ}\text{C/s}$  to about  $30^{\circ}\text{C/s}$ , the ellipse ratio displayed an almost linear increase from values of around 2 to those of about 2.5, which indicated a tendency for the second-phase particles to become progressively more elongated, and these values were found to be similar for both the recrystallised and deformed starting austenite. At a cooling rate of around  $100^{\circ}\text{C/s}$ , the ellipse ratio of the M/A particles for the recrystallised prior austenite abruptly increased to a value of 3.3, which was significantly larger than that of 2.4 obtained for the deformed austenite (see Fig. 6b). This is consistent with the microstructure dominated by BF in the former case as opposed to that largely composed of GF in the latter case, as discussed above.

Figure 7 shows the volume fraction of second-phase particles, calculated with respect to the entire microstructure, as a function of cooling rate for the transformation products formed from the both recrystallised and deformed austenite. The corresponding curves displayed a similar shape, starting with the values of around 12% at a cooling rate of  $0.1^{\circ}\text{C/s}$  and reaching a minimum at values of

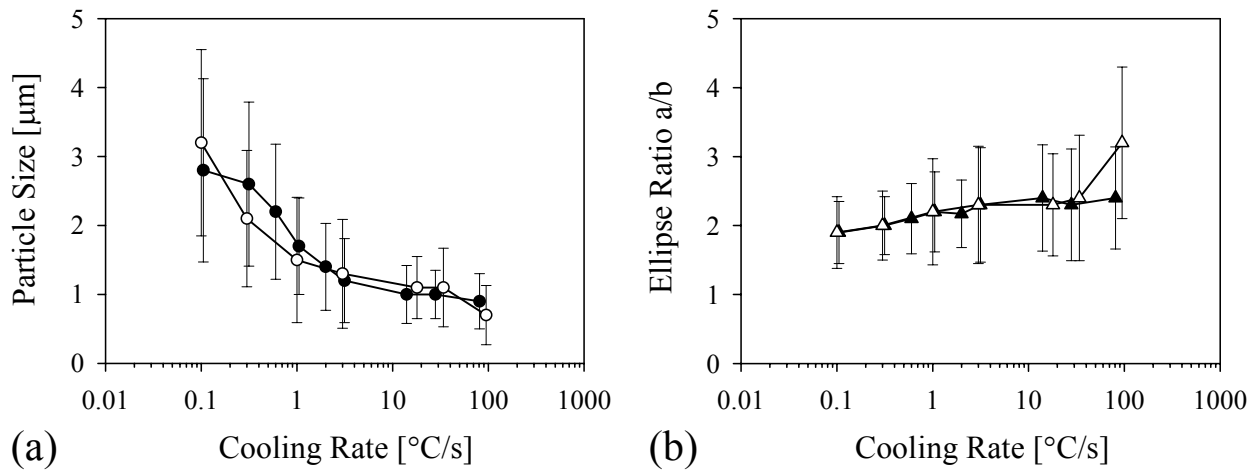


Fig. 6. Results of a statistical analysis of the second-phase particle parameters as a function of cooling rate: (a) mean size; (b) mean shape expressed using the ellipse ratio a/b (open and filled symbols correspond to the recrystallised and deformed starting austenite, respectively; error bars indicate standard deviations from the mean values).

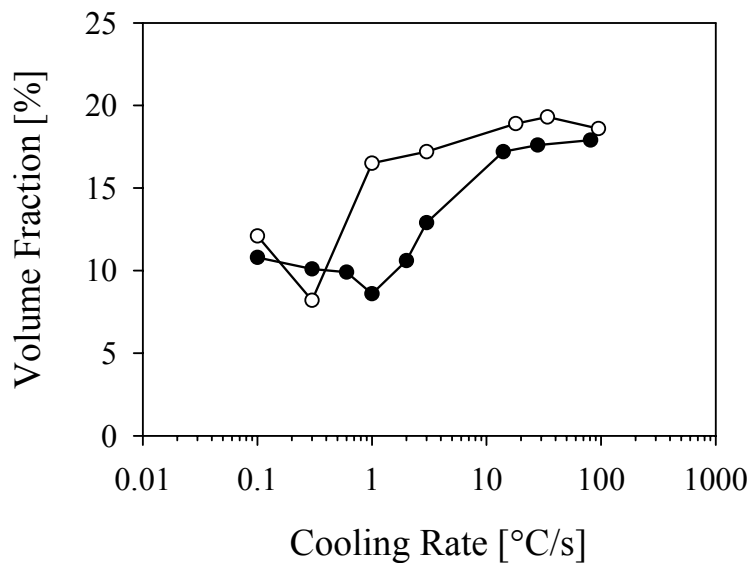


Fig. 7. Volume fraction of the second-phase particles as a function of cooling rate (open and filled symbols correspond to the recrystallised and deformed starting austenite, respectively).

about 8%, followed by a step rise to a plateau characterised by values of around 18% at high cooling rates. The curve for the deformed austenite was shifted towards the lower volume fraction values and higher cooling rates with respect to its counterpart corresponding to the recrystallised starting matrix. The above shift seems to reflect that shown by the respective CCT diagrams (see Fig. 2), caused by reduced effective hardenability of the deformed prior austenite. The observed decrease of the second-phase volume fraction towards the minimum with increasing cooling rate reflects the transition from the microstructures characterised by coarse classical bainite particles embedded within the PF matrix to those comprised of GF sheaves, which contained classical bainite particles, and PF grains. The subsequent rise in the volume fraction values with increasing cooling rate reflects a gradual transition from the microstructures partly containing (progressively finer) classical bainite particles to those containing exclusively M/A micro-regions.

### 3. DISCUSSION

#### 3.1. TRANSFORMATION BEHAVIOUR

Heavy deformation of austenite, carried out at a temperature (875°C) situated below the non-recrystallisation limit, resulted in a pronounced shift of the PF transformation field in the CCT diagram towards higher cooling rates (see Fig. 2), which is in good correspondence with the published data [2,6,7]. The observed enhanced formation of PF may be attributed to both an increase in the austenite stored energy due to plastic deformation and a concomitant rise in the density of ferrite nucleation sites, as well as to the lowering of the amount of Nb in solid solution due to strain-induced precipitation of Nb carbonitrides, which decreases austenite hardenability [6]. It is well known that the presence of PF in the microstructure of high-strength pipeline steels needs to be minimised [1]. From the inspection of the CCT diagrams in Fig. 2 it follows that, in the present case, the minimum cooling rate values required to avoid PF formation were around 1°C/s and 10°C/s for transformation from the recrystallised and deformed austenite respectively. It is necessary to note that both the above values, the latter one in particular, might be slightly higher in the industrial processing of similar steels due to both a finer prior austenite grain size and a larger amount of strain within the austenite, known to decrease steel hardenability. Once the cooling rate exceeded the above limits, PF formation was avoided and a variety of non-equilibrium ferrite microstructures was obtained. In contrast to PF, the transformation characteristics of these non-equilibrium transformation products generally appeared less sensitive to deformation of the parent austenite in the steel investigated (see Fig. 2), which is in agreement with findings presented in [7,8].

#### 3.2. TRANSFORMATION MICROSTRUCTURES

The formation of PF grains, characterised by rather low internal dislocation densities, was accompanied by the presence of carbon-enriched austenite regions, stabilized against further PF formation. This was a result of the carbon content of the steel that exceeded the solubility limit in PF. The carbon-enriched austenite was found to subsequently undergo complex decomposition during further cooling, presumably due to variation in carbon enrichment. Small fractions of P or P', observed within the carbon-enriched islands at the very low cooling rates, suggest that the pearlite transformation field was occasionally intersected in some local volumes during cooling. The bulk of the carbon-rich austenite transformed into a mix of BII and BIII types of classical bainite [5]. As already mentioned above, the presence of larger amounts of PF in the microstructure of the pipeline steels should be avoided [1]. This is for the reason that PF is detrimental to strength, as documented by the hardness values presented in Fig. 2, and also brings about discontinuous yielding that might cause some problems during pipe forming due to the Bauschinger phenomenon [1,3].

Unlike the PF grains described above, the non-equilibrium ferrite microstructures were generally observed to contain significant internal dislocation densities, which is consistent with continuous yielding displayed by these transformation products [1-3]. It seems reasonable to suggest that the increased dislocation densities found within both QF grains and GF or BF sheaves/packets originated mainly from accommodation of the stresses, caused by a volume change accompanying the transformation at the relatively low temperatures involved. The frequently observed low-angle boundaries, subdividing the above grains or sheaves/packets into smaller fragments, appear to have largely resulted from mutual impingement of several growing ferrite crystals, formed by separate nucleation events or sympathetically [9]. Consequently, it could be expected that some carbon-

enriched austenite regions, stabilized against further transformation to ferrite, might become entrapped locally between the growing non-equilibrium ferrite crystals. Indeed, such local volumes, transformed during subsequent cooling to either bainite or M/A micro-constituents, were frequently observed in the present study. On the basis of careful comparisons of the ferrite microstructures classified as QF or GF in the present work with those available in the literature, it appears that these constituents might essentially be products of WF transformation, undergoing some subsequent degeneration [9,10]. A possible reason why QF requires relatively higher temperatures for its formation compared to GF has been suggested in [10]. The results of the present investigation suggest that BF might perhaps represent a genuine “bainitic” microstructure, alternatively classified as BI carbide-free upper bainite, having a different formation mechanism [5].

The non-equilibrium ferrite microstructures are known to contribute to an increase in strength, through small effective grain size, increased dislocation densities and dispersion of second-phase hard particles, while maintaining a reasonable level of toughness [1-3]. For the microstructures comprised of a mixture of GF and QF, increased volume fraction of GF accompanying increase in cooling rate was observed to gradually enhance strength, as indicated by the hardness values presented in Fig. 2, whereas toughness is expected to decrease. When the cooling rate was high enough for BF to be formed, the strength was further increased (see Fig. 2) but the toughness is known to deteriorate [3]. Thus, the results of the present study indicate that, through a careful control of continuous cooling, microstructures with a balance of properties potentially suitable for higher-grade pipeline steel development can be obtained.

#### 4. CONCLUSIONS

The transformation behaviour and transformation product microstructures have been studied in an API X80 pipeline steel during simulated recrystallisation and non-recrystallisation controlled rolling, followed by controlled cooling at rates from 0.1°C/s to about 100°C/s. Deformation dilatometry in conjunction with advanced metallographic techniques were employed in the investigation and the corresponding CCT diagrams were constructed. It was observed that severe plastic deformation of the parent austenite markedly enhanced PF formation indicating a significant effective decrease in austenite hardenability. In contrast, the non-equilibrium ferrite microstructures, classified as QF, GF and BF, generally appeared less sensitive to deformation of the parent austenite in the steel investigated. The detailed transformation and microstructural characteristics, obtained in the present work, could be used for the optimisation of thermomechanical processing schedules for API X80 and similar higher-grade pipeline steels.

#### REFERENCES

- 1) J.G. WILLIAMS, C.R. KILLMORE, F.J. BARBARO, A. META and L. FLETCHER, Proc. Int. Conf. Microalloying'95, Pittsburgh (1995), TMS, Warrendale, USA (1995), p. 117.
- 2) I. TAMURA, H. SEKINE, T. TANAKA and CH. OUCHI, Thermomechanical Processing of High-Strength Low-Alloy Steels. Butterworths, London (1988), 248pp.
- 3) B.P. WYNNE, P. CIZEK, C.H.J. DAVIES, B.C. MUDDLE and P.D. HODGSON, Proc. Int. Conf. THERMEC'97, Wollongong (1997), TMS, Warrendale, USA (1997), p. 837.
- 4) T. ARAKI, Atlas for Bainitic Microstructures Vol. 1. Continuous-Cooled Microstructures of Low-Carbon Steels. Iron Steel Inst. Jpn., Tokyo (1992), 165pp.
- 5) Y. OHMORI and T. MAKI, Mater. Trans. JIM 32, (1991), p. 631.
- 6) P.A. MANOHAR, T. CHANDRA and C.R. KILLMORE, Iron Steel Inst. Jpn. Int. 36, (1996), p. 1486.

- 7) P. CIZEK, B.P. WYNNE, C.H.J. DAVIES, B.C. MUDDLE and P.D. HODGSON, Metall. Mater. Trans. 33A, (2002), p. 1331.
- 8) H. TAMEHIRO, M. MURATA and R. HABU, Proc. Int. Conf. HSLA Steels'85, Beijing (1985), ASM Intern., Metals Park, Ohio (1986), p. 325.
- 9) G. SPANOS and M.G. HALL, Metall. Mater. Trans. 27A, (1996), p. 1519.
- 10) S. OKAGUCHI, H. OHTANI and Y. OHMORI, Mater. Trans. JIM 32, (1991), p. 697.